CellPress

Chemistry & Biology
Article

Reprogramming Acyl Carrier Protein Interactions of an Acyl-CoA Promiscuous *trans*-Acyltransferase

Zhixia Ye,[1] Ewa M. Musiol,[2,3,4] Tilmann Weber,[2,3,4] and Gavin J. Williams[1,*]
[1]Department of Chemistry, North Carolina State University, Raleigh, NC 27695-8204, USA
[2]Interfaculty Institute of Microbiology and Infection Medicine, Eberhard Karls University of Tübingen, Auf der Morgenstelle 28, 72076 Tübingen, Germany
[3]German Center for Infection Research (DZIF), Partner Site Tübingen, Tübingen, Germany
[4]Present address: The Novo Nordisk Foundation Center for Biosustainability of the Technical University of Denmark (DTU), 2970 Hørsholm, Denmark
*Correspondence: gavin_williams@ncsu.edu
http://dx.doi.org/10.1016/j.chembiol.2014.02.019

SUMMARY

Protein interactions between acyl carrier proteins (ACPs) and *trans*-acting acyltransferase domains (trans-ATs) are critical for regioselective extender unit installation by many polyketide synthases, yet little is known regarding the specificity of these interactions, particularly for trans-ATs with unusual extender unit specificities. Currently, the best-studied trans-AT with nonmalonyl specificity is KirCII from kirromycin biosynthesis. Here, we developed an assay to probe ACP interactions based on leveraging the extender unit promiscuity of KirCII. The assay allows us to identify residues on the ACP surface that contribute to specific recognition by KirCII. This information proved sufficient to modify a noncognate ACP from a different biosynthetic system to be a substrate for KirCII. The findings form a foundation for further understanding the specificity of trans-AT:ACP protein interactions and for engineering modular polyketide synthases to produce analogs.

INTRODUCTION

The scaffolds of a variety of clinically relevant natural products are biosynthesized by polyketide synthases (PKSs). Type I PKSs are organized in a modular fashion, whereby each module is responsible for the installation of an extender unit acyl-coenzyme A (CoA) into the growing polyketide (Staunton and Weissman, 2001). The growing chain and all other substrates are covalently tethered to the phosphopantetheinyl prosthetic arm of acyl carrier proteins (ACPs), located within each module. Acyltransferase (AT) domains are required to select extender units and attach them to an ACP, whereas ketosynthase (KS) domains catalyze C-C bond formation to extend the growing polyketide. Modifications to this basic paradigm can be found in natural biosynthetic systems. For example, fungal PKSs are type I PKSs that act iteratively, whereby a given module catalyzes several extender unit installations (Cox and Simpson, 2009). In most type I PKSs, the AT domains are embedded within each module and are *cis*-acting. In contrast, a growing number of PKSs are being discovered that house ATs external to the modules (Cheng et al., 2003; Piel, 2010). Such *trans*-acting ATs (trans-ATs) at the genetic level can be easily transferred between biosynthetic systems. Subsequently, given their discrete nature, trans-ATs might constitute a valuable alternative to strategies that involve *cis*-acting AT (cis-AT) domain swapping, and there is much interest in developing trans-ATs for use as tools in synthetic biology platforms aimed at the regioselective modification of polyketides (Kumar et al., 2003; Walker et al., 2013). For example, promiscuity of KSs from the 6-deoxyerythronolide synthase (DEBS) toward diverse extender units (Koryakina et al., 2013a; Sundermann et al., 2013) could be harnessed by trans-ATs that display acyl-CoA specificity orthogonal to that of the DEBS cis-AT domains, yet one critical barrier to the use of trans-ATs as tools for polyketide diversification is our poor understanding of extender unit and ACP specificity. For example, the native substrate for many trans-ATs is malonyl-CoA (Figure 1), and these enzymes are unlikely to display activity toward other acyl-CoAs (Koryakina et al., 2013b). Furthermore, whereas some trans-ATs that use malonyl-CoA install the extender unit at multiple positions within the resulting polyketide and are ACP promiscuous (Wong et al., 2010), others install unusual extenders at limited positions in the polyketide and are likely ACP specific (Figure 1) (Liu et al., 2009; Musiol et al., 2011; Zhao et al., 2010). Thus, the ACP specificity of trans-ATs needs to be better understood so that specificity can be manipulated. Although evidence of the ability to manipulate ACP interactions with other domains is emerging (Haines et al., 2013; Kapur et al., 2010, 2012), little is known regarding trans-AT:ACP interactions. Indeed, including the malonyl-CoA-ACP transacylase (MCAT) that primarily serves ACPs from type II fatty acid synthases, only two trans-AT structures are available (Keatinge-Clay et al., 2003; Wong et al., 2011), in addition to that of a bifunctional trans-AT/decarboxylase (Lohman et al., 2013). Docking models have helped propose the ACP interaction epitopes of MCAT and at least one genuine malonyl-CoA specific trans-AT (Arthur et al., 2009; Keatinge-Clay et al., 2003; Wong et al., 2011), and NMR studies have also contributed to this picture (Arthur et al., 2009).

Recently, we probed the promiscuity of several trans-ATs toward a panel of acyl-CoAs (Koryakina et al., 2013b). One target, KirCII from kirromycin biosynthesis (Figure 2), is responsible for installation of the C28 ethyl moiety of kirromycin, via

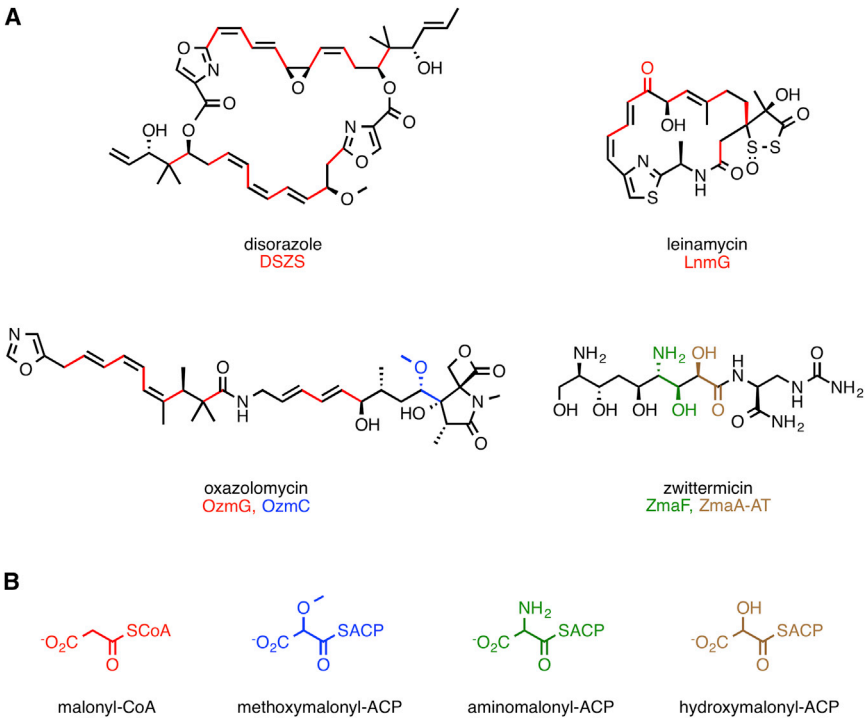

Figure 1. Substrate Specificity of Trans-ATs

(A) Examples of polyketides biosynthesized via trans-ATs. The contribution of each trans-AT and the corresponding substrate are shown color coded.

(B) Examples of acyl-thioester substrates for trans-ATs.

ethylmalonyl-CoA (Musiol et al., 2011). KirCII has the distinction of being the only characterized trans-AT to naturally utilize a nonmalonyl acyl-CoA substrate (Musiol and Weber, 2012). All other unusual trans-AT extender units are introduced into polyketides linked to ACPs (Figure 1). Our study led to the discovery that in addition to ethylmalonyl-CoA, KirCII can utilize other acyl-CoAs, making KirCII the most promiscuous trans-AT known. Kirromycin biosynthesis involves the action of another trans-AT (KirCI) responsible for malonyl installation onto ACPs within 11 unique modules of the kirromycin biosynthetic assembly line (Musiol et al., 2013). According to this biosynthetic logic, it is likely that the acyl-CoA and ACP specificity of KirCII is orthogonal to that of KirCI. This feature would present a valuable opportunity to elucidate the molecular basis for ACP specificity of a uniquely acyl-CoA promiscuous trans-AT. Here, we describe a cycloaddition assay to rapidly characterize and probe KirCII:ACP interactions, which led to characterization of the ACP specificity of KirCII and promoted identification of the KirCII:ACP interaction epitope. This information allowed us to successfully convert a noncognate ACP into a substrate for KirCII via a single amino acid mutation. The insight into trans-AT:ACP interactions obtained here will contribute to improving trans-AT-based strategies for polyketide diversification.

RESULTS

Cycloaddition Assay for Probing KirCII:ACP Interactions

The ability of KirCII to utilize extender unit acyl-CoAs modified with azide/alkynyl functionality could enable the quantification of KirCII activity via bioorthogonal ligation chemistry and in-gel fluorescence detection (Figure 3A). In-gel fluorescence detection of KirCII-catalyzed *trans*-acylation of holo-ACP5$_{Kir}$ was evaluated using azidoethylmalonyl-CoA (AzEM-CoA) as substrate and strain-promoted azide-alkyne cycloaddition using a commercially available dibenzocyclooctyne (DIBO)-Alexa Fluor 647 conjugate. Upon fluorescence visualization of a SDS-PAGE gel, a distinct band was observed at a position corresponding to the loaded ACP5$_{Kir}$ (Figure 3B). In the absence of KirCII, acyl-CoA, or cyclooctyne-fluorophore, only background signal was detected. As expected, activity was not detected when apo-ACP5$_{Kir}$ was used in place of holo-ACP5$_{Kir}$. Furthermore, Sfp was used to transfer the azido-functionalized phosphopantetheine moiety from AzEM-CoA to apo-ACP5$_{Kir}$, resulting in strong labeling with the cyclooctyne-fluorophore (Figure 3B). Next, the fluorescence intensity of the labeled ACP bands was quantified by in-gel fluorescence analysis. Inclusion of the MCAT from *Streptomyces coelicolor* or the malonyl-CoA trans-AT from the disorazole synthase (DSZS), which cannot utilize AzEM-CoA, in place of KirCII failed to produce labeled ACP (Figure 3C). In addition, the fluorescence intensity was shown to be dependent on the KirCII reaction incubation time (Figure 3D) and the concentration of KirCII (Figure 3E). Cumulatively, these data show that AzEM-CoA and cycloaddition enable the rapid and efficient quantification of KirCII activity.

ACP Specificity of KirCII

Previous studies led to the conclusion that KirCII is responsible for installation of the C29-ethyl moiety in kirromycin (Musiol et al., 2011). Given the presence of another trans-AT in the kirromycin biosynthetic gene cluster, we set out to investigate whether KirCII displays specificity for ACP5$_{Kir}$ or whether KirCII could potentially interact with other ACPs from kirromycin biosynthesis. Each kirromycin ACP was subcloned into an expression plasmid as an N-terminal His$_6$-tagged fusion protein, fully converted to the holo-ACP, and subsequently purified to homogeneity (see Supplemental Information available online). The conversion of each apo-ACP to the holo-form was monitored by liquid chromatography-mass spectrometry (MS) analysis of the reaction mixtures, which indicated that in every case, conversion was 100% (Figure S1). Each holo-ACP was then tested as a substrate for KirCII-catalyzed *trans*-acylation using AzEM-CoA (Figure 4). In this assay, ACP5$_{Kir}$ supported the highest activity with KirCII, although ACP0$_{Kir}$, ACP3$_{Kir}$, and ACP7$_{Kir}$ supported basal activity at 15%–25% of ACP5$_{Kir}$. The

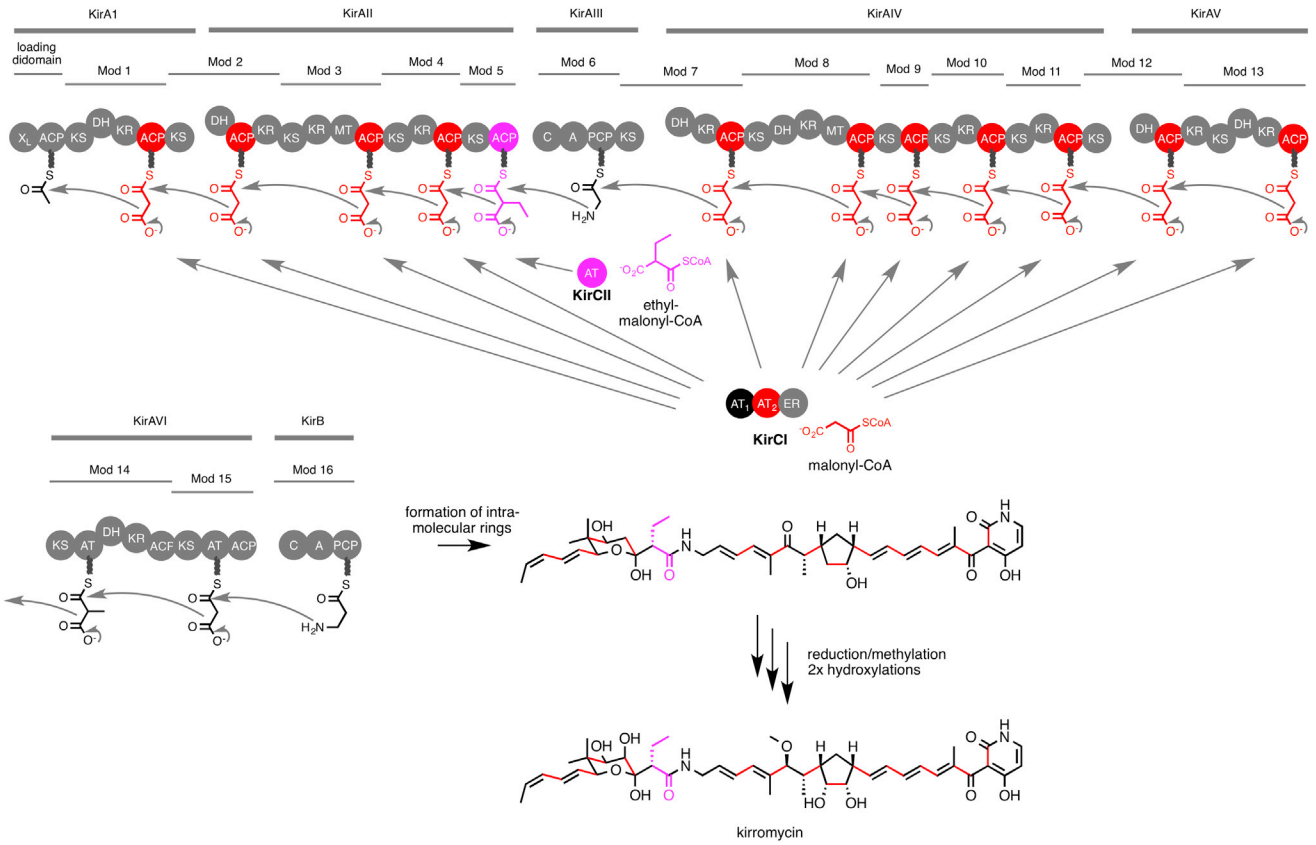

Figure 2. Biosynthesis of Kirromycin
The putative biosynthetic contribution of KirCI (malonyl-CoA, red) and KirCII (ethylmalonyl-CoA, purple) to the final structure of kirromycin is highlighted.

remainder of the ACPs tested displayed activities that were <10% of $ACP5_{Kir}$. These data suggest that $ACP5_{Kir}$ is the preferred interaction partner for KirCII, and other kirromycin ACPs are poor substrates for KirCII. The ACP specificity of KirCII supports a role for programmed protein interactions in maintenance of kirromycin biosynthetic fidelity.

Mapping the KirCII:$ACP5_{Kir}$ Interaction Epitope

The ACP specificity of KirCII led us to speculate that $ACP5_{Kir}$ interacts with KirCII through a set of unique residues at the ACP surface. Accordingly, we set out to map this epitope via alanine scanning mutagenesis. In order to identify residues predicted to be surface exposed, a homology model for $ACP5_{Kir}$ was constructed using the SWISS-MODEL workspace and the apo-D-alanyl carrier protein as template (Protein Data Bank code 1DV5) (see Experimental Procedures for details). A total of 61 (non-Ala/Gly) surface residues were then individually mutated to Ala, expressed, subjected to Sfp-mediated phosphopantetheinylation, and purified. Notably, three of these mutants, D64A, L66A, and I83A, could not be completely converted to the holo-form, whereas L52A, L58A, Y79A, F88A, and T93A could not be expressed in soluble form. D64 and L66 are immediately adjacent to the presumed phosphopantetheinylation site (S65), and mutations at this position in other ACPs are known to hinder modification by Sfp (Weissman et al., 2006). The I83A mutant is largely unfolded, as judged by analysis of the corresponding CD spectrum. Thus, these eight mutants were omitted from further analysis. The CD spectra of a representative panel of the $ACP5_{Kir}$ mutants matched very closely to that of wild-type (WT) $ACP5_{Kir}$, indicating similar secondary structures (Figure S2). Next, each $ACP5_{Kir}$ mutant was tested as a substrate for KirCII using AzEM-CoA and the cycloaddition assay. Many of the mutants displayed activity similar to WT $ACP5_{Kir}$, indicating that mutation to Ala at these positions does not significantly impact interaction with KirCII (Figure 5A). However, substitution at five positions (H44, L45, R51, D60, and R70) resulted in activities <20% of that of the WT $ACP5_{Kir}$ with KirCII (Figure 5A). The locations of these five positions were mapped onto the $ACP5_{Kir}$ model (Figure 5B), which begins to define at least part of the interaction epitope. In addition to those residues identified from alanine scanning mutagenesis, the well-known and highly conserved DSL motif comprising $ACP5_{Kir}$ residues D64, S65, and L66 (see Table S1 for a list of carrier protein residues involved in various protein interactions) can likely be included in this epitope, given that the phosphopantetheinylation site is embedded within this motif and previous experimental evidence (Weissman et al., 2006).

Computational Docking

To provide further insight into the molecular basis of the KirCII ACP specificity, a homology model for KirCII was obtained using the SWISS-MODEL workspace (Arnold et al., 2006).

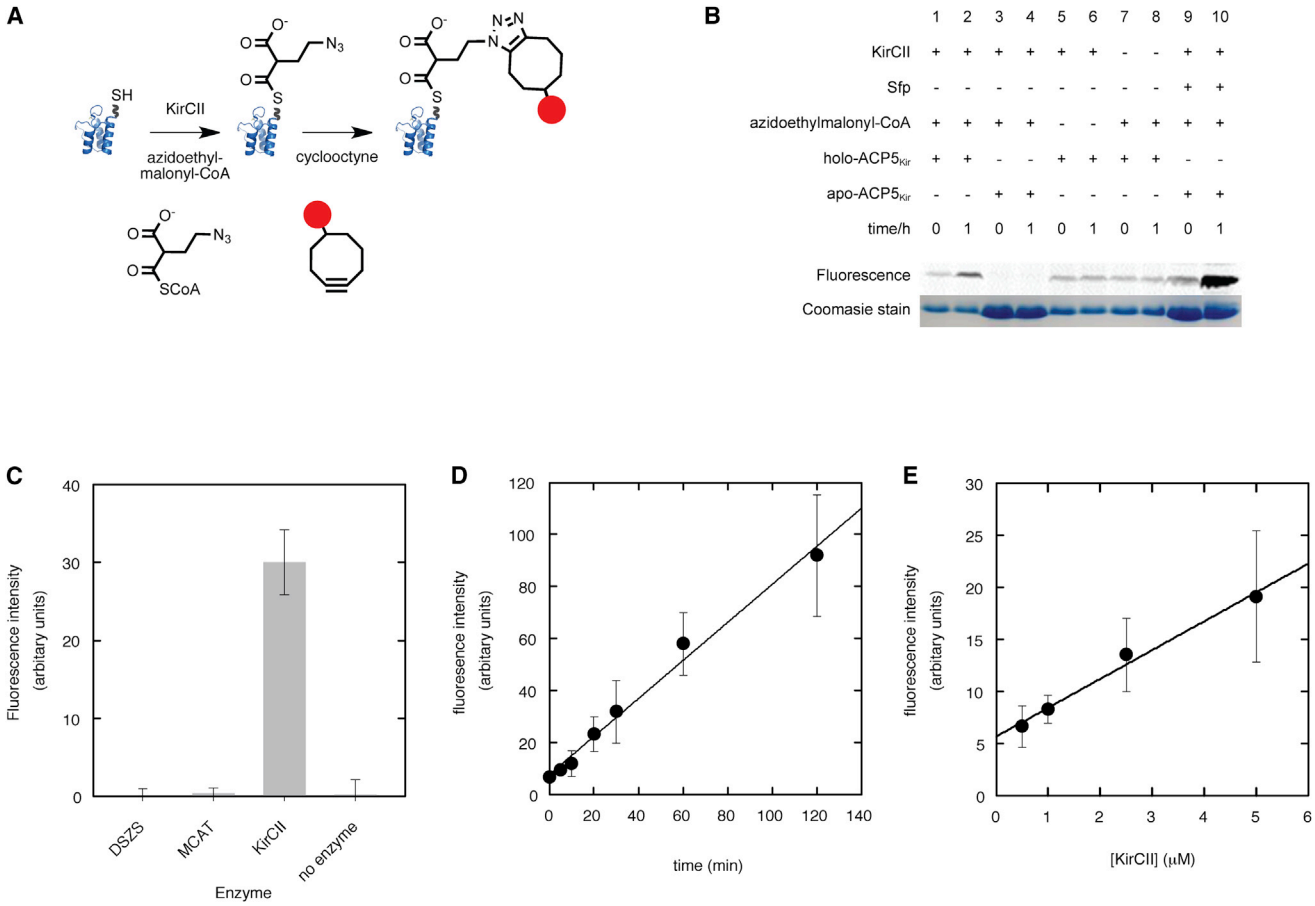

Figure 3. Cycloaddition Assay for KirCII:ACP Interactions

(A) KirCII-catalyzed *trans*-acylation and subsequent cycloaddition.

(B) In-gel fluorescence detection of a series of KirCII control assays. Coomassie blue image shows ACP loading in each reaction.

(C) Fluorescence intensity of labeled $ACP5_{Kir}$ in a series of control reactions using various trans-ATs or no enzyme.

(D) Fluorescence intensity of KirCII-labeled $ACP5_{Kir}$ as a function of time.

(E) Fluorescence intensity of labeled $ACP5_{Kir}$ as a function of KirCII concentration. Error bars represent the SD of the mean (n = 2).

Interestingly, the natively *cis*-acting [KS3][AT3] di-domain from DEBS (34% identity to KirCII) was selected by SWISS-MODEL as the template. Although KirCII functionally resembles the trans-ATs DSZS and MCAT, the crystal structures of which are known (Keatinge-Clay et al., 2003; Wong et al., 2011), these two structures were not selected by SWISS-MODEL, likely because of poor sequence identity with KirCII (27% and 22% sequence identity to KirCII, respectively). This is in agreement with phylogenetic analyses, which showed that KirCII is more closely related to cis-ATs than to malonate-specific trans-ATs (Musiol and Weber, 2012). In addition to the large and small AT subdomains typical of trans-ATs, the modeled KirCII structure also includes a KS-AT linker domain that is usually associated with *cis*-acting AT domains from type I PKSs (Liew et al., 2012; Tang et al., 2006). This prediction is in agreement with the sequence length of KirCII (which is longer than that of DSZS and MCAT), homology between the N-terminal portion of KirCII and various cis-ATs (Figure S3), and secondary structure similarity between the predicted KirCII KS-AT linker and structure of a known linker domain (Figure S4). The KS-AT linker domain was included in our subsequent protein interaction studies, given the possibility that the linker region participates in ACP recognition by *cis*-acting AT domains. Furthermore, the KS-AT linker domain appears important for solubility of KirCII, given that a truncated version of KirCII that lacks the linker could not be expressed in soluble form. The PatchDock (Schneidman-Duhovny et al., 2005) and the ClusPro (Kozakov et al., 2013) servers were then used for molecular docking simulations using the $ACP5_{Kir}$ and KirCII models. Gratifyingly, both servers converged on almost identical docking results, without any physical constraints. One of the top models was chosen on the basis of the alanine scanning mutagenesis data described above (Figure 6A). Overall, the docking model resembles that of the iterative type I PKS DynE8 AT and ACP (Liew et al., 2012) and also that of the AT3-ACP3 model from DEBS (Wong et al., 2010). $ACP5_{Kir}$ is predicted to sit in a large cleft formed by parts of the KS-AT linker domain, as well as the small and large subdomains. Gratifyingly, this model places the ACP phosphopantetheine attachment site (S65) ~20 Å away from the presumed active site catalytic Ser (S203) of KirCII, and an active site tunnel can be identified that

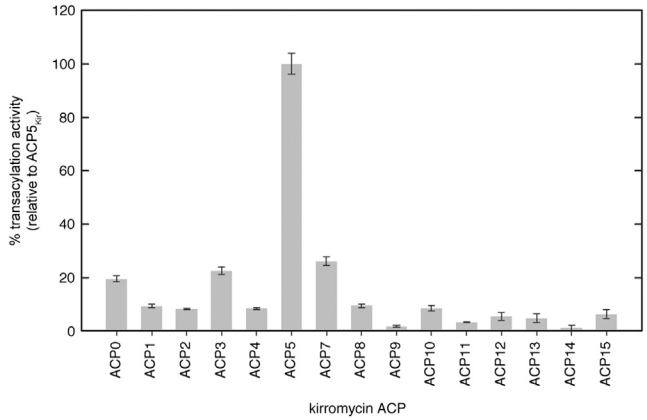

Figure 4. ACP Specificity of KirCII

Activity of 3 μM KirCII with 30 μM each kirromycin ACP and 300 μM AzEM-CoA was determined by the cycloaddition assay. Error bars represent the SD of the mean (n = 2).

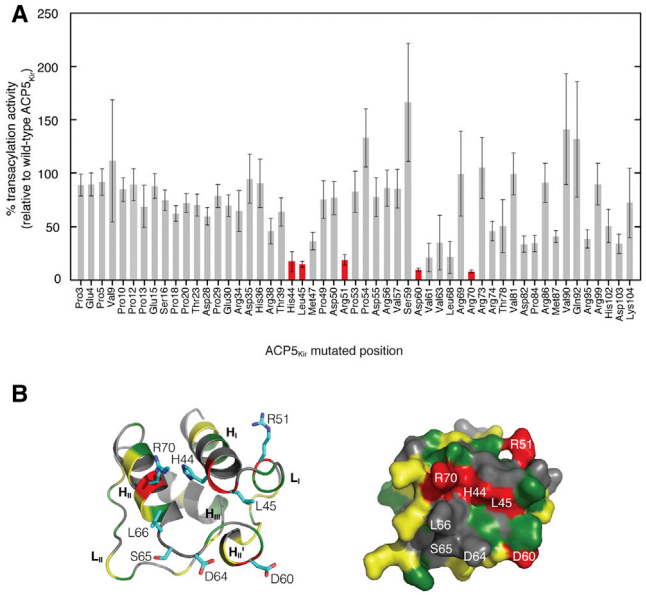

Figure 5. Mapping the KirCII:ACP Interaction Epitope by Alanine Scanning Mutagenesis

(A) *trans*-Acylation rates of holo-ACP5$_{Kir}$ alanine mutants with KirCII. Rates are expressed as percentages of the activity with wild-type ACP5$_{Kir}$. Wild-type positions that were Ala/Gly were not mutated. Mutants that displayed <20% the activity of the wild-type holo-ACP5$_{Kir}$ are highlighted red.

(B) *trans*-Acylation activities of ACP5$_{Kir}$ alanine mutants mapped onto an ACP5$_{Kir}$ homology model ribbon diagram (left panel) and its computed surface (right panel). Red, <20% activity; green, 20%–80% activity; yellow, >80% activity; gray, not determined. Error bars represent the SD of the mean (n = 2).

could accommodate the requisite ACP phosphopantetheine. This model positions each of the five residues identified from alanine scanning mutagenesis (H44, L45, R51, D60, and R70) intimately at the interface between the ACP and KirCII. For example, the carboxylate side chain of D60 of ACP5$_{Kir}$ is predicted to make a salt bridge with the terminus of the R410 side chain of KirCII (Figure 6A). Interestingly, docking models of the DynE8 AT:ACP (Liew et al., 2012), DEBS AT4:ACP4 (Tang et al., 2006), and fungal nonreducing PksA:ACP complexes (Bruegger et al., 2013), also implicate an Asp equivalent to D60 of ACP5$_{Kir}$ at the interface (Table S1). Notably, D60, along with the nearby D64, appear to form a negatively charged group of residues in loop I (L_1) of ACP5$_{Kir}$ that interacts with three consecutive Arg residues from KirCII (R408–R410). Positively charged residues of other ATs are often involved in ACP interactions with an Asp residue analogous to ACP5$_{Kir}$ D64 (Keatinge-Clay et al., 2003; Liew et al., 2012; Tang et al., 2006, 2007). In addition, ACP5$_{Kir}$ R51 and R70, both judged as important for interaction with KirCII by alanine scanning mutagenesis, are positioned to interact with D98 and E395 of KirCII, respectively. Further, the main chain nitrogen of ACP5$_{Kir}$ A48 is positioned for hydrogen bonding with the hydroxyl of KirCII Y426. Another key predicted interaction involves E245 and R69 from KirCII and ACP5$_{Kir}$, respectively (Figure 6A). To test the accuracy of this model, a series of KirCII mutants was constructed and assayed by using the cycloaddition assay and ACP5$_{Kir}$ as substrate. The secondary structure of each mutant matched closely to that of WT KirCII, as judged by CD spectroscopy (Figure S5). The KirCII mutants R408A, R409A, and R410A supported *trans*-acylation at slightly lower rates compared with WT KirCII with ACP5$_{Kir}$ as substrate (Figure 6B). Moreover, substitution of each Arg with Glu further reduced the activity of each mutant. In addition, a triple mutant where all three Arg residues (R408–R410) were mutated to Ala displayed less than 10% *trans*-acylation activity compared with wild-type KirCII, whereas no activity was detected for when all three arginines were mutated to Glu (Figure 6B). These results suggest that KirCII R408–R410 play a significant role in the interaction with ACP5$_{Kir}$. Similarly, mutation of D98 of KirCII to Ala reduced activity to just 30% of the WT KirCII activity (Figure 6B). Mutation of E245 to Ala reduced activity in comparison to WT KirCII, whereas activity could not be detected when the same residue was substituted with Arg (Figure 6B). Substitution of KirCII E395 with Ala resulted in loss of activity, whereas substitution with Arg completely abolished activity. Similarly, the predicted importance of Y426 of KirCII was confirmed by mutagenesis (Figure 6B). These data are consistent with the electrostatic contributions of these residues predicted on the basis of the docking model and suggest that this set of residues is important for controlling interactions between KirCII and ACP5$_{Kir}$. Finally, two surface residues more distant from the predicted interface were also targeted. Substitution of D123 with Ala resulted in a slight increase in activity with ACP5$_{Kir}$ as substrate, whereas substitution of the same residue with Arg resulted in ~50% *trans*-acylation activity, compared with WT KirCII (Figure 6B). Meanwhile, substitution of E170 with Ala resulted in small decrease in activity with ACP5$_{Kir}$ as substrate, and substitution of E170 with Arg resulted in ~50% *trans*-acylation activity, compared with WT KirCII, (Figure 6B). Thus, substitution of negatively charged residues distal from the predicted interface with a neutral amino acid has a small effect compared with equivalent substitutions at predicted interface residues. Similarly, substitution at these distal sites with oppositely charged residues results in only ~2-fold decreased activity, compared with wild-type KirCII, whereas such substitutions at residues predicted to be involved in the KirCII epitope (e.g., R408E, R409E, R410E, and E245R) led to dramatic decreases in activity compared with

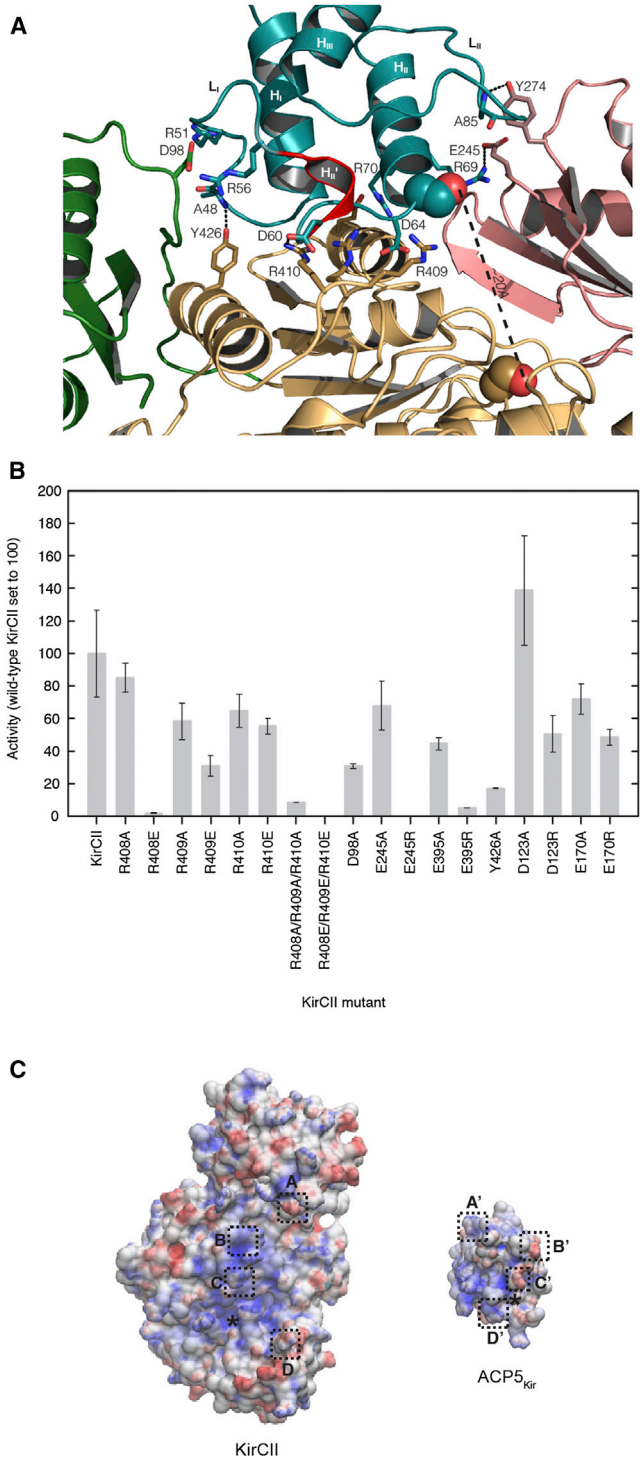

Figure 6. Docking Model of the KirCII:ACP5$_{Kir}$ Interaction

(A) A homology model for ACP5$_{Kir}$ was used as a ligand to dock with a homology model for KirCII. See Experimental Procedures for details regarding generation of the homology models. The KirCII large subdomain is shown in light orange, the small subdomain of KirCII is shown in light pink, the KirCII linker domain is green, and ACP5$_{Kir}$ is shown in teal. The H_{II}' portion of L_I of ACP5$_{Kir}$ is highlighted red. Phosphopantetheinylation site of ACP5$_{Kir}$ and the KirCII catalytic Ser are shown as spheres. For clarity, not every highlighted residue is labeled.

(B) Mutational analysis of KirCII putative interface residues. Error bars represent the SD of the mean (n = 2).

(C) Electrostatic surface potential maps of KirCII and ACP5$_{Kir}$ are calculated using the PDB2PQR server (Dolinsky et al., 2007). Colors range from blue (positive) to white (neutral) to red (negative). Four key electrostatic contacts are shown boxed; the KirCII contacts are shown with boxes A (D98), B (R410), C (R409), and D (E245), whereas those of ACP5$_{Kir}$ are shown with boxes A′ (R51), B′ (D60), C′ (D64), and D′ (R69). The asterisk indicates the position of the KirCII active site Ser and the ACP5$_{Kir}$ phosphopantetheinylation site. The surfaces are represented so that if ACP5$_{Kir}$ is rotated 180°, the letters from each surface would match.

wild-type KirCII. Cumulatively, these data suggest that several electrostatic interactions contribute to molecular recognition between KirCII and its cognate ACP. Electrostatic surface maps of KirCII and ACP5$_{Kir}$ highlight the charge complementarity between several regions of the predicted interface (Figure 6C).

Mutagenesis of a Noncognate ACP

The docking model and mutagenesis data described above suggest that a portion of L_1, several C-terminal residues of helix I (H_I), and N-terminal residues of helix II (H_{II}) are each involved in the KirCII interaction epitope, whereas loop II (L_{II}) and helix III (H_{III}) of ACP5$_{Kir}$ do not make significant contributions to the interaction with KirCII. To test this hypothesis and to further define the ACP sequence elements required for ACP specificity of KirCII, chimeras between ACP5$_{Kir}$ and a noncognate ACP from kirromycin biosynthesis were constructed (Figures 7A and 7B). ACP10$_{Kir}$ was selected to contribute to these chimeras, because this ACP shares the highest amino acid sequence identity (35%) to ACP5$_{Kir}$ among the kirromycin ACPs. Notably, the entire N-terminal half (L_0-H_I-L_I) of ACP5$_{Kir}$ is sufficient to provide robust recognition by KirCII when fused with the C-terminal portion (H_{II}-L_{II}-H_{III}-L_{III}) of ACP10$_{Kir}$. The corresponding chimera, ACP10$_{Kir}$ NA5, supported 50% activity compared with the WT ACP5$_{Kir}$, a 5-fold improvement in efficiency compared with the noncognate ACP (Figure 7B). In contrast, the reverse chimera that includes the N-terminal portion of ACP10$_{Kir}$ and the C-terminal portion of ACP5$_{Kir}$ displays no detectable activity with KirCII (compare ACP10$_{Kir}$ NA5 and ACP10$_{Kir}$ CA5, Figure 7B). These data suggest that the majority of the ACP5$_{Kir}$:KirCII recognition features are located in the N-terminal L_0-H_I-L_I portion of ACP5$_{Kir}$, in agreement with the docking model and alanine scanning mutagenesis results. In an attempt to further refine the putative interaction epitope, a series of chimeras was designed that exchanged individual secondary structure elements. Exchange of ACP10$_{Kir}$ H_I or L_I with the corresponding structural element from ACP5$_{Kir}$ each led to a 2-fold improvement in activity, compared with the WT ACP10$_{Kir}$ (Figure 7B), and could not therefore recapitulate the full activity of the ACP10$_{Kir}$ NA5 chimera that contained the entire N-terminal portion of ACP5$_{Kir}$. Interestingly, preceding H_I of each kirromycin ACP is a short sequence labeled L_0 that is predicted to form a random coil (Figure S6). As judged by sequence homology, this sequence element is not equivalent to the docking domains postulated to play some role in protein interactions between other trans-ATs and ACPs (Tang et al., 2004) (data not shown). Substitution of the ACP10$_{Kir}$ L_0 region with that from ACP5$_{Kir}$ failed to significantly alter ACP specificity (see ACP10$_{Kir}$ L0A5; Figure 7B), whereas deletion of L_0 from ACP5$_{Kir}$ resulted in an insoluble protein.

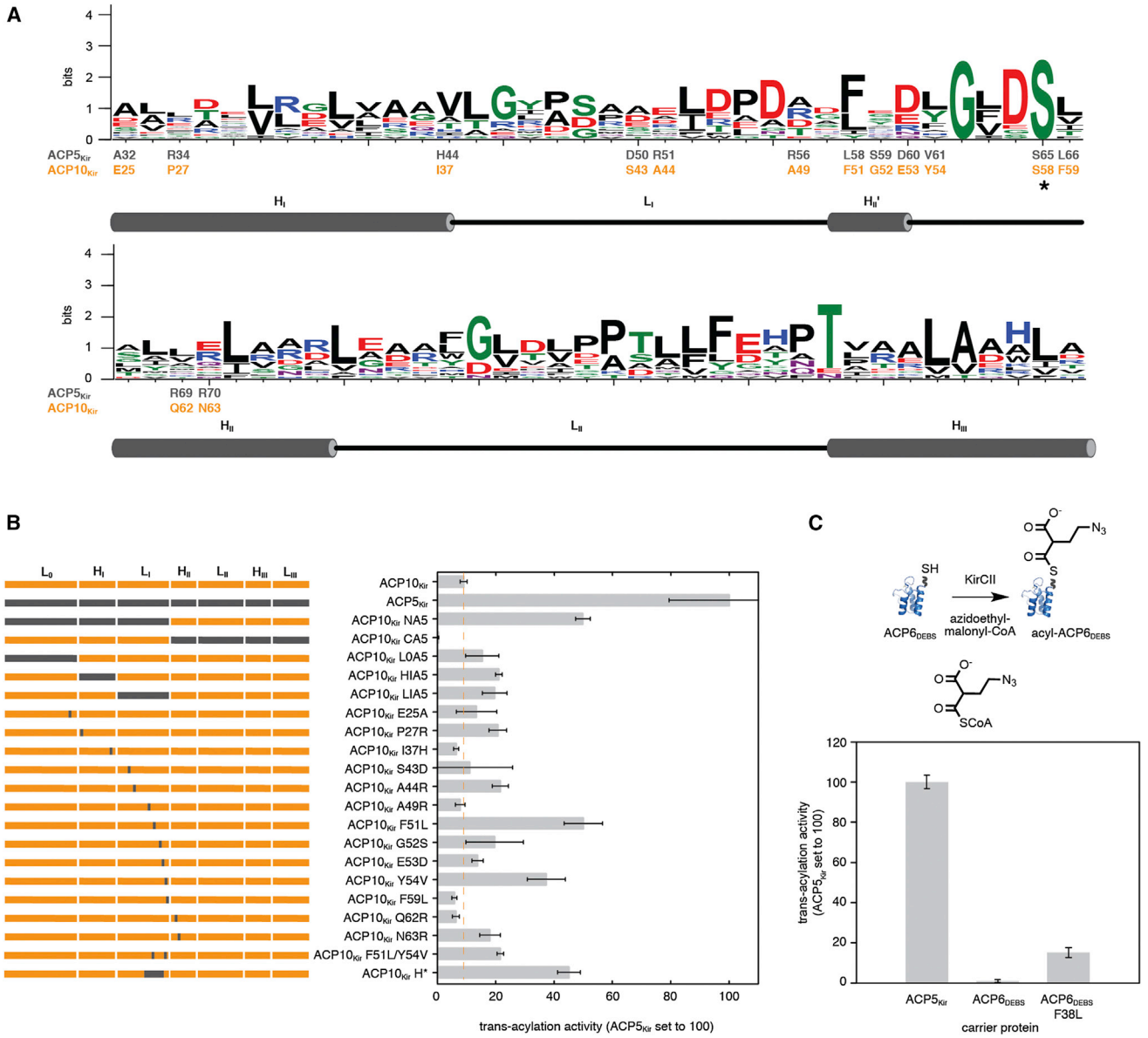

Figure 7. Probing the ACP:KirCII Interaction Epitope by Mutagenesis of a Noncognate ACP

(A) Sequence logo for the kirromycin ACPs. Shown in gray and orange, respectively, are the amino acids at selected positions of $ACP5_{Kir}$ and $ACP10_{Kir}$. The asterisk indicates the phosphopantetheinylation site. Positions discussed in the text are highlighted. Boundaries between each secondary structure element are also shown. For brevity, N- and C-terminal loop regions (L_0 and L_{III}) are not shown. L_0 is the region preceding H_I, and L_{III} is the region following H_{III}.

(B) Scheme showing contribution of $ACP5_{Kir}$ and $ACP10_{Kir}$ to each chimera or mutant (left panel), and activities of WT, chimeric, and mutant kirromycin ACPs with KirCII (right panel). The rates are expressed as percentages of the activity with WT holo-$ACP5_{Kir}$.

(C) Activities of WT and mutant $ACP6_{DEBS}$ with KirCII, expressed as percentages of the activity with WT holo-$ACP5_{Kir}$. See Experimental Procedures for reaction and assay conditions. Error bars represent the SD of the mean (n = 2).

Interestingly, many residues within H_I, L_I, and H_{II} of $ACP5_{Kir}$/$ACP10_{Kir}$ are poorly conserved among kirromycin ACPs, as judged by alignment of their amino acid sequences (Figure 7A and Figure S7). Moreover, four of these poorly conserved positions correspond to residues that were previously highlighted by alanine scanning mutagenesis of $ACP5_{Kir}$ (H44, R51, D60, and R70). Accordingly, we hypothesized that some of these poorly conserved residues, perhaps including some from the alanine scanning mutagenesis set, might dictate the ACP specificity of KirCII. To test the contribution of these poorly conserved positions in controlling specificity, a panel of 13 mutants was constructed that substituted each selected residue within H_I, L_I, and H_{II} of $ACP10_{Kir}$ with the corresponding residue from $ACP5_{Kir}$ (Figure 7A). With respect to positions highlighted by alanine scanning mutagenesis, substitution at I37 and E53 in $ACP10_{Kir}$ (equivalent to H44 and D60 in $ACP5_{Kir}$, Figure 7A) provided only small changes to the *trans*-acylation activity, compared with wild-type $ACP10_{Kir}$ (see I37H and E53D,

Figure 7B). In contrast, the $ACP10_{Kir}$ mutants A44R and N63R (corresponding to positions R51 and R70 in $ACP5_{Kir}$, Figure 7A) each display approximately 2-fold higher activity with KirCII, compared with wild-type $ACP10_{Kir}$, underscoring the importance of these two previously highlighted positions for recognition by KirCII. Interestingly, substitution of $ACP10_{Kir}$ Q62 with Arg (equivalent to R69 in $ACP5_{Kir}$) failed to improve activity with KirCII, compared with WT $ACP10_{Kir}$, even though this residue is adjacent to the equivalent of R70 in $ACP5_{Kir}$. This result is entirely consistent with the alanine scanning mutagenesis data, which show that of the R69/R70 pair in $ACP5_{Kir}$, only substitution at R70 is detrimental to activity with KirCII. Presumably, R70 in $ACP5_{Kir}$ contributes more to the interaction with KirCII than the neighboring R69, even though R69 is predicted to interact with KirCII via E245 (Figures 6A–6C). Perhaps mutation to Ala at R69 can be better compensated by other side chain rearrangements than Ala substitution at R70. Notably, aside from $ACP5_{Kir}$, Arg is never found at residue 69 among the kirromycin ACPs, and this residue is most frequently Leu or Val (Figure 7A and Figure S7). Similarly, at residue 70, Arg is found only three times among all 15 kirromycin ACP sequences and is most often the oppositely charged Glu (Figure 6A and Figure S7). The most active $ACP10_{Kir}$ single amino acid exchanges were those at positions F51 and Y54 (equivalent to L58 and V61 in $ACP5_{Kir}$) and do not correspond to positions highlighted by our alanine scanning mutagenesis. Substitution at these two positions with the equivalent residue from $ACP5_{Kir}$, Leu and Val, respectively, supported activity 5-fold higher than WT $ACP10_{Kir}$ (Figure 7B). Consistent with these data, mutagenesis of the $ACP5_{Kir}$ residue corresponding to $ACP10_{Kir}$ Y54 resulted in a mutant that showed only 21% the activity of WT $ACP5_{Kir}$ ($ACP5_{Kir}$ V61A; Figure 5A). Intriguingly, the $ACP5_{Kir}$ residue equivalent to $ACP10_{Kir}$ F51 (L58) was not expressed in soluble form when mutated to Ala as part of the previous surface mutagenesis and was therefore not highlighted by the surface mutagenesis data. Interestingly, $ACP5_{Kir}$ L58 and V61 are not well conserved among the kirromycin ACPs (Figure 7A and Figure S7). For example, residue 58 is most often Phe (as in $ACP10_{Kir}$ F51) and is Leu in only four of the kirromycin ACP sequences. Residue 61 is usually Leu or Tyr (as in $ACP10_{Kir}$ Y54) among the kirromycin ACPs and is Val only in $ACP5_{Kir}$. Combination of both F51L and Y54V in $ACP10_{Kir}$ actually resulted in a slight decrease in *trans*-acylation activity compared with either the F51L or Y54V mutant (Figure 7B). However, exchange of a portion of a L_I sequence in $ACP10_{Kir}$ that included F51 and Y54 with that from $ACP5_{Kir}$ (H_{II}', corresponding to V57–D60 in $ACP5_{Kir}$), resulted in a chimera with 5-fold the activity of wild-type $ACP10_{Kir}$ ($ACP10_{Kir}$-H*; Figure 7B). Thus, the precise identities of residues within this short helix are critical for maintaining maximal activity with KirCII. Together, these data suggest that in $ACP5_{Kir}$, Arg residues at positions 51/70 and Leu/Val at positions 58/61, respectively, are required but not totally sufficient for recognition by KirCII.

Reprogramming KirCII Interactions toward a Noncognate ACP from the Erythromycin PKS

Some trans-ATs have been shown to be promiscuous toward the ACP substrate and can utilize ACPs from different biosynthetic pathways (Walker et al., 2013; Wong et al., 2010). The conclusions that Arg is required at positions 51/70 of $ACP5_{Kir}$ and that Leu and Val are required at positions 58 and 61 led us to predict whether ACPs from other biosynthetic systems would serve as substrates for KirCII. For example, ACP6 from DEBS includes Asp and Gly at positions equivalent to 51/70 of $ACP5_{Kir}$, whereas at residues equivalent to $ACP5_{Kir}$ 58 and 61, Phe and Leu are present in the $ACP6_{DEBS}$, respectively. Accordingly, we predicted that $ACP6_{DEBS}$ would not serve as an efficient substrate for KirCII. This hypothesis was tested by carrying out the cycloaddition assay using AzEM-CoA, KirCII, and holo-$ACP6_{DEBS}$. As predicted, WT holo-$ACP6_{DEBS}$ was not a detectable substrate for KirCII (Figure 7C). Given that the $ACP10_{Kir}$ mutation F51L led to improved *trans*-acylation activity with KirCII (Figure 7B), compared with the wild-type $ACP10_{Kir}$, and that the equivalent residue in $ACP6_{DEBS}$ is also Phe (F38), we proposed that introduction of leucine at position 38 of $ACP6_{DEBS}$ would improve the *trans*-acylation efficiency of this noncognate ACP with KirCII. To test this notion, the mutant $ACP6_{DEBS}$ F38L was constructed, converted to the holo-form, and assayed with KirCII. Remarkably, and in complete contrast to wild-type $ACP6_{DEBS}$, the F38L mutant was a detectable substrate for KirCII, and this substitution improved *trans*-acylation activity at least 14-fold compared with WT $ACP6_{DEBS}$ (Figure 7C). This shows that the activity of a trans-AT has been rationally engineered toward a noncognate carrier protein.

DISCUSSION

An improved understanding of protein interactions is required to overcome limitations related to the ACP specificity of trans-ATs. Although structural studies of trans-ATs that utilize malonyl-CoA have slowly emerged (Keatinge-Clay et al., 2003; Wong et al., 2011), nothing is known regarding the structure and ACP interactions of trans-ATs with unusual acyl-CoA specificities. In this study, we harnessed the acyl-CoA promiscuity of KirCII (Koryakina et al., 2013b) to rapidly probe its interaction with a series of ACPs. The expected cognate protein, $ACP5_{Kir}$, was found to be the preferred substrate for KirCII, whereas the enzyme was capable of utilizing other kirromycin ACPs to a lesser extent. These data suggest that programmed protein interactions could play a role in controlling extender unit incorporation into kirromycin but do not rule out the role of downstream substrate specificity or editing functions.

The specificity of KirCII for $ACP5_{Kir}$, coupled with the relatively high sequence homology between the other kirromycin ACPs, provided an opportunity to identify ACP elements that contribute to trans-AT specificity. Alanine scanning mutagenesis identified several ACP residues that, when mutated to Ala, almost completely abolished activity with KirCII. Interestingly, this result contrasts with alanine scanning mutagenesis of the malonyl-CoA specific, yet ACP promiscuous trans-AT, DSZS (Wong et al., 2011), which revealed only two positions that were sensitive to substitution. Computational prediction of the interaction between $ACP5_{Kir}$ and KirCII provided a model that was consistent with the alanine scanning mutagenesis data. The KS-AT linker domain, the large AT subdomain, and small AT subdomain of KirCII are all predicted to be involved in ACP recognition. The KS-AT linker domain of KirCII may contribute to the strict ACP specificity of KirCII, given that structures of the ACP promiscuous trans-ATs MCAT and DSZS do not include this domain. In

fact, R51 of $ACP5_{Kir}$, which interacts with the linker domain in the model (Figure 6A), is most often Glu or Ala in other ACPs. Furthermore, the position equivalent to $ACP5_{Kir}$ R51 in other ACPs is not predicted to be involved in interactions with trans-ATs or other interacting domains (Table S1). Additional $ACP5_{Kir}$ residues that appear to contribute to recognition by KirCII that are also not identified by other protein interaction studies include R56 and R70. Notably though, some predicted KirCII:$ACP5_{Kir}$ interactions involve ACP residues that have been implicated in other protein interaction studies. For example, D64 is part of the highly conserved DSL motif and is predicted to be involved in diverse interactions between various PKS domains. Another key residue, D60, is often Asp or Glu in other ACPs and has been implicated in protein interactions between other ATs. Curiously, D60 locates to a short helical turn (H_{II}' in Figures 5B and 6A) in the middle of L_I of $ACP5_{Kir}$. Intriguingly, short helical turns similar to H_{II}' have been proposed to contribute to other ACP interactions. For example, a short helix located within L_{II} has been proposed to flag ACPs for β-branching in polyketide biosynthesis (Haines et al., 2013). In another example, a similarly short helical turn was implicated in the specific interaction between the curacin A ACP_I and halogenase embedded within the CurA module (Busche et al., 2012). Further, in the nonreducing PKS PksA ACP, an aspartate equivalent to $ACP5_{Kir}$ D60, located in a small helical turn, is predicted to make a key electrostatic interaction with the KS domain of PksA (Bruegger et al., 2013). Notably, we found that recognition by KirCII was very sensitive to amino acid substitution in the H_{II}' region of $ACP5_{Kir}$. Individual substitutions at two key hydrophobic sites in this region were sufficient to improve the activity of $ACP10_{Kir}$ 5-fold with KirCII. Moreover, we established that amino acid substitution at one site within this region of an ACP from an entirely different biosynthetic system was sufficient to convert a completely inactive ACP into a robust substrate. Thus, the overall shape, position of D60, or dynamics of the H_{II}' region may be important for specifying the activity of a given ACP with KirCII. In fact, hydrophobic packing within a similar short helical turn of ACP-mupA3a from mupirocin biosynthesis was recently found to contribute significantly to recognition by the cognate *trans*-acting β-branching domain, MupH (Haines et al., 2013). In addition to our extensive mutagenesis of the kirromycin ACPs, the role of several KirCII residues was probed by substituting key charged residues with neutral or oppositely charged amino acids. The results were consistent with the docking model and suggested that charged residues at the KirCII:$ACP5_{Kir}$ interface contribute to the strict ACP specificity of KirCII by forming key electrostatically matched interactions. Furthermore, these data suggest that KirCII harnesses a larger number of electrostatic interactions with its cognate ACP than that of ACP promiscuous trans-ATs such as MCAT and DSZS. Thus, a picture is emerging whereby the ACP specificity of KirCII is a consequence of a large and unique set of charged and hydrophobic residues at the $ACP5_{Kir}$ surface. Together, these data describe the interaction epitope between a non-malonyl-utilizing trans-AT and cognate ACP.

Critically, those $ACP5_{Kir}$ residues involved in recognition by KirCII would have been difficult to identify from sequence analysis alone. For example, several charged $ACP5_{Kir}$ residues that are poorly conserved among the kirromycin ACPs are not important for KirCII specificity (e.g., R34, D35, and R38). Similarly, a pair of Arg residues in H_{II} of $ACP5_{Kir}$ (R73/R74) are quite conspicuous and might have been assumed to be important for KirCII recognition by comparison to other kirromycin ACPs, yet neither residue was found to be important herein.

Cumulatively, our data provide a platform for harnessing the acyl-CoA promiscuity of KirCII for diversification of polyketides. For example, with knowledge of the $ACP5_{Kir}$:KirCII epitope in hand, ACPs from other biosynthetic systems might now be identified by sequence comparison that could be recognized by KirCII. In addition, the insight obtained here will enable strategies for further engineering trans-AT:ACP interactions. It is envisioned that residues in noncognate ACPs that correspond to those recognized by KirCII (or other trans-ATs) could be targeted for mutagenesis and screening or selection, by utilizing the cycloaddition assay in combination with cell surface display.

SIGNIFICANCE

Trans-ATs offer exciting possibilities for polyketide diversification, especially given the potential extender unit promiscuity of KS domains (Koryakina et al., 2013a). However, little is known regarding the ACP or extender unit specificity of many trans-ATs. Putative ACP recognition features have emerged only with those trans-ATs that naturally utilize malonyl-CoA, with limited potential to introduce other extender units into polyketides. Understanding the features of ACPs that allow recognition by a cognate trans-AT is a crucial first step that may enable manipulation of trans-AT ACP specificity. We proposed that the trans-AT KirCII only interacts with a single ACP within the parent kirromycin biosynthetic assembly line, and this would provide an opportunity to probe the ACP features required for recognition by a uniquely acyl-CoA promiscuous trans-AT. We recognized that the ability of KirCII to utilize substrates modified with chemical handles for click chemistry could be leveraged to provide a rapid and convenient assay for measuring the activity of KirCII. Accordingly, the activity of KirCII toward each kirromycin ACP was measured, providing evidence that KirCII interacts specifically with the expected cognate ACP. A combination of ACP surface mutagenesis, docking simulations, KirCII mutagenesis, and substitutions of amino acids and structural elements led to the identification of several key electrostatic interactions that define the $ACP5_{Kir}$:KirCII interaction epitope. Remarkably, this insight enabled engineering a completely noncognate ACP into a detectable substrate for KirCII via the introduction of a single amino acid substitution. Our data combined with previous studies highlight the importance of small helical turns located within loop regions that connect the larger helices that form the basis of all ACP structures. In the long term, an improved understanding of the features that allow recognition of an ACP by trans-ATs can be used as a foundation for designing strategies that allow the diversification of polyketides.

EXPERIMENTAL PROCEDURES

General

Unless otherwise stated, all materials and reagents were of the highest grade possible and purchased from Sigma. Isopropyl β-D-thiogalactoside (IPTG)

was from. Bacterial strain *Escherichia coli* BL21(DE3) competent cells were from Promega. Primers were ordered from Integrated DNA Technologies. Analytical high-performance liquid chromatography (HPLC) was performed on a Varian ProStar system.

Cloning and Expression of Kirromycin ACPs

The genes encoding kirromycin ACPs were amplified from cosmids 1C24 and 2C23 (Weber et al., 2008) using HotStar HiFidelity polymerase (QIAGEN) and the primers listed in Table S2. Fragments were cloned in pET30Ek/LIC (Novagen/Merck Millipore) using the manufacturer's protocol. Plasmids harboring each kirromycin ACP were cotransformed with plasmid pSU20-Sfp into *E. coli* BL21(DE3). A single colony was then used to inoculate 3 ml of Luria Burtani (LB) medium containing 34 μg/ml chloramphenicol and 50 μg/ml kanamycin that was cultured overnight at 37°C with shaking at 250 rpm. The overnight culture was used to inoculate 300 ml of LB medium containing the same antibiotics and was then incubated at 37°C at 250 rpm until the optical density 600 had reached ~0.6. Protein expression was induced by the addition of 0.5 mM IPTG and was then incubated at 18°C at 250 rpm for 18 hr. MS analysis of initial trials indicated that in vivo phosphopantetheinylation yielded significant but incomplete conversion to the holo-form. To drive phosphopantetheinylation to completion, an in vitro conversion to the holo-form was also performed using cleared cell extract from each ACP overexpression. Briefly, cleared cell extract prepared from 300 ml of cell culture was mixed with 40 μl of 50 mM CoA and was incubated at room temperature for 4 hr and then kept at 4°C overnight. The proteins were then purified by nickel-nitrilotriacetic acid chromatography largely as previously described (Musiol et al., 2013), except the batch purification method was used. MS analysis showed full conversion to the holo ACP for every ACP (Figure S1).

Cloning and Expression of Sfp, KirCII, DSZS, and MCAT

Cloning and expression of Sfp, KirCII, DSZS, and MCAT were performed as previously described (Koryakina et al., 2013b).

Chemoenzymatic Synthesis of Azidoethylmalonyl-CoA

Chemoenzymatic synthesis of azidoethylmalonyl-CoA was performed in 400 μl of reaction mixture containing 100 mM sodium phosphate (pH 7), $MgCl_2$ (2 mM), ATP (6 mM), coenzyme A (3 mM), azidoethyl malonate (15 mM) (Koryakina et al., 2013b), and mutant MatB (20 μg) at 25°C. Production of azidoethylmalonyl-CoA was confirmed by HPLC. Aliquots were removed after overnight incubation, quenched with an equal volume of ice-cold methanol, and centrifuged at 10,000 × *g* for 10 min, and cleared supernatants were used for HPLC analysis on a Varian ProStar HPLC system. A series of linear gradients was developed from 0.1% trifluoroacetic acid (A) in water to methanol (HPLC grade, B) using the following protocol: 0–32 min, 80% B; 32–35 min, 100% A. The flow rate was 1 ml/min, and the absorbance was monitored at 254 nm using Pursuit XRs C18 column (250 mm × 4.6 mm; Varian).

General Procedure for Strain-Promoted Azide-Alkyne Cycloaddition Assay

The strain-promoted azide-alkyne cycloaddition assay was performed in a total volume of 6 μl and contained 4 μl of KirCII assay mixture containing 20 μM $ACP5_{Kir}$ and 2 μl of 600 μM of DIBO-Alexa Fluor 647 (Life Technologies). The reaction was incubated in dark at room temperature with gentle agitation for 1 hr. The reactions were boiled after addition of protein loading dye for 5 min before analysis by SDS-PAGE. The gels were scanned using a Typhoon 7000 phosphoimager to determine the intensity of DIBO-labeled proteins bands. The bands were quantified by ImageQuant TL software (GE Life Sciences), and the rubber-band background subtraction method was applied.

KirCII Titration Assay

KirCII titration assay was performed in 10 μl of reaction mixture containing 50 mM Tris-HCl (pH 7.5), 50 mM $MgCl_2$, 300 μM of azidoethylmalonyl-CoA, 50 μM holo $ACP5_{Kir}$, and KirCII at room temperature for 20 min. 4 μl of KirCII reaction mixture was then removed for strain-promoted azide-alkyne cycloaddition assay.

KirCII Time-Course Assay

KirCII time-course assay was performed in 70 μl of reaction mixture containing 50 mM Tris-HCl (pH 7.5), 50 mM $MgCl_2$, 300 μM of azidoethylmalonyl-CoA, 30 μM holo $ACP5_{Kir}$, and 1 μM KirCII at room temperature. Aliquots were removed at different time points and stored at −80°C before being used for strain-promoted azide-alkyne cycloaddition assay.

Alanine Scanning Mutagenesis of $ACP5_{Kir}$

Primers for alanine scanning mutagenesis of $ACP5_{Kir}$ were designed with lengths between 25 and 30 bp, whereas melting temperatures were between 70°C and 75°C. Site-directed mutagenesis was performed following the QuikChange protocol (Agilent Technologies).

KirCII assay using each $ACP5_{Kir}$ alanine scanning mutant was performed in 10 μl of reaction mixture containing 50 mM Tris-HCl (pH 7.5), 50 mM $MgCl_2$, 300 μM of azidoethylmalonyl-CoA, 30 μM holo $ACP5_{Kir}$, and 3 μM KirCII at room temperature for 1 hr. An aliquot (4 μl) of the reaction mixture was then removed and assayed using the strain-promoted azide-alkyne cycloaddition procedure.

Circular Dichroism

Circular dichroism (CD) measurements were performed with a JASCO 810 CD Spectropolarimeter. Samples for CD were buffer exchanged into CD buffer (10 mM potassium phosphate, 50 mM sodium sulfate, pH 7.4), and the concentration of samples was 0.2 mg/ml. Spectra from 190 to 260 nm were scanned at a step of 0.5 nm at 20°C in a 0.1-cm cuvette, with ten repeats. The scan speed was 100 nm/min.

Homology Model of $ACP5_{Kir}$ and KirCII

Homology models for $ACP5_{Kir}$ and KirCII were generated using the automated mode of the SWISS-MODEL workspace (http://swissmodel.expasy.org/). The template used for $ACP5_{Kir}$ was PDB ID 1DV5 (Volkman et al., 2001), and the sequence identity between the template and $ACP5_{Kir}$ was 26%. The template for KirCII was PDB ID 2QO3 (Tang et al., 2007), and the sequence identity between template and KirCII was 34%. Based on QMEAN z scores (Benkert et al., 2011), the quality for the homology models is good.

Site-Directed Mutagenesis and Chimeragenesis of ACPs and KirCII

Plasmid pET30-KirACP10 was used as a template for mutagenesis of $ACP10_{Kir}$. For mutagenesis of KirCII, plasmid pET52-KirCII was used (Musiol et al., 2011). ACP and KirCII amino acid substitutions were performed using the QuikChange protocol (Agilent Technologies). Multiple-template-based sequential PCR (Shan and Lynch, 2010) was used for construction of ACP chimeras. *E. coli* DH5α was used for plasmid amplification. All mutations were confirmed by DNA sequencing. Specific primer sequences used for construction of $ACP10_{Kir}$/$ACP5_{Kir}$ chimeras can be found in the supplemental information (Table S3).

SUPPLEMENTAL INFORMATION

Supplemental Information includes seven figures and three tables and can be found with this article online at http://dx.doi.org/10.1016/j.chembiol.2014.02.019.

ACKNOWLEDGMENTS

This study was supported by an NSF CAREER award (CHE-1151299 to G.J.W.), NIH grant GM104258-01 (to G.J.W.), and a Faculty Research and Professional Development award from North Carolina State University (to G.J.W.). T.W. was supported by the German Center for Infection Research. The authors thank Christopher Ladner for helpful discussions and the Biological Core Instrumentation Facility in the Department of Chemistry at North Carolina State.

Received: December 23, 2013
Revised: January 27, 2014
Accepted: February 6, 2014
Published: April 10, 2014

REFERENCES

Arnold, K., Bordoli, L., Kopp, J., and Schwede, T. (2006). The SWISS-MODEL workspace: a web-based environment for protein structure homology modelling. Bioinformatics *22*, 195–201.

Arthur, C.J., Williams, C., Pottage, K., Płoskoń, E., Findlow, S.C., Burston, S.G., Simpson, T.J., Crump, M.P., and Crosby, J. (2009). Structure and malonyl CoA-ACP transacylase binding of Streptomyces coelicolor fatty acid synthase acyl carrier protein. ACS Chem. Biol. *4*, 625–636.

Benkert, P., Biasini, M., and Schwede, T. (2011). Toward the estimation of the absolute quality of individual protein structure models. Bioinformatics *27*, 343–350.

Bruegger, J., Haushalter, B., Vagstad, A., Shakya, G., Mih, N., Townsend, C.A., Burkart, M.D., and Tsai, S.C. (2013). Probing the selectivity and protein·protein interactions of a nonreducing fungal polyketide synthase using mechanism-based crosslinkers. Chem. Biol. *20*, 1135–1146.

Busche, A., Gottstein, D., Hein, C., Ripin, N., Pader, I., Tufar, P., Eisman, E.B., Gu, L., Walsh, C.T., Sherman, D.H., et al. (2012). Characterization of molecular interactions between ACP and halogenase domains in the curacin A polyketide synthase. ACS Chem. Biol. *7*, 378–386.

Cheng, Y.Q., Tang, G.L., and Shen, B. (2003). Type I polyketide synthase requiring a discrete acyltransferase for polyketide biosynthesis. Proc. Natl. Acad. Sci. USA *100*, 3149–3154.

Cox, R.J., and Simpson, T.J. (2009). Fungal type I polyketide synthases. Methods Enzymol. *459*, 49–78.

Dolinsky, T.J., Czodrowski, P., Li, H., Nielsen, J.E., Jensen, J.H., Klebe, G., and Baker, N.A. (2007). PDB2PQR: Expanding and upgrading automated preparation of biomolecular structures for molecular simulations. Nucleic Acids Res. *35*, W522–W525.

Haines, A.S., Dong, X., Song, Z., Farmer, R., Williams, C., Hothersall, J., Płoskoń, E., Wattana-amorn, P., Stephens, E.R., Yamada, E., et al. (2013). A conserved motif flags acyl carrier proteins for β-branching in polyketide synthesis. Nat. Chem. Biol. *9*, 685–692.

Kapur, S., Chen, A.Y., Cane, D.E., and Khosla, C. (2010). Molecular recognition between ketosynthase and acyl carrier protein domains of the 6-deoxyerythronolide B synthase. Proc. Natl. Acad. Sci. USA *107*, 22066–22071.

Kapur, S., Lowry, B., Yuzawa, S., Kenthirapalan, S., Chen, A.Y., Cane, D.E., and Khosla, C. (2012). Reprogramming a module of the 6-deoxyerythronolide B synthase for iterative chain elongation. Proc. Natl. Acad. Sci. USA *109*, 4110–4115.

Keatinge-Clay, A.T., Shelat, A.A., Savage, D.F., Tsai, S.C., Miercke, L.J., O'Connell, J.D., 3rd, Khosla, C., and Stroud, R.M. (2003). Catalysis, specificity, and ACP docking site of Streptomyces coelicolor malonyl-CoA:ACP transacylase. Structure *11*, 147–154.

Koryakina, I., McArthur, J.B., Draelos, M.M., and Williams, G.J. (2013a). Promiscuity of a modular polyketide synthase towards natural and non-natural extender units. Org. Biomol. Chem. *11*, 4449–4458.

Koryakina, I., McArthur, J., Randall, S., Draelos, M.M., Musiol, E.M., Muddiman, D.C., Weber, T., and Williams, G.J. (2013b). Poly specific trans-acyltransferase machinery revealed via engineered acyl-CoA synthetases. ACS Chem. Biol. *8*, 200–208.

Kozakov, D., Beglov, D., Bohnuud, T., Mottarella, S.E., Xia, B., Hall, D.R., and Vajda, S. (2013). How good is automated protein docking? Proteins *81*, 2159–2166.

Kumar, P., Koppisch, A.T., Cane, D.E., and Khosla, C. (2003). Enhancing the modularity of the modular polyketide synthases: transacylation in modular polyketide synthases catalyzed by malonyl-CoA:ACP transacylase. J. Am. Chem. Soc. *125*, 14307–14312.

Liew, C.W., Nilsson, M., Chen, M.W., Sun, H., Cornvik, T., Liang, Z.X., and Lescar, J. (2012). Crystal structure of the acyltransferase domain of the iterative polyketide synthase in enediyne biosynthesis. J. Biol. Chem. *287*, 23203–23215.

Liu, T., Huang, Y., and Shen, B. (2009). Bifunctional acyltransferase/decarboxylase LnmK as the missing link for beta-alkylation in polyketide biosynthesis. J. Am. Chem. Soc. *131*, 6900–6901.

Lohman, J.R., Bingman, C.A., Phillips, G.N., Jr., and Shen, B. (2013). Structure of the bifunctional acyltransferase/decarboxylase LnmK from the leinamycin biosynthetic pathway revealing novel activity for a double-hot-dog fold. Biochemistry *52*, 902–911.

Musiol, E.M., and Weber, T. (2012). Discrete acyltransferases involved in polyketide biosynthesis. MedChemComm *3*, 871–886.

Musiol, E.M., Härtner, T., Kulik, A., Moldenhauer, J., Piel, J., Wohlleben, W., and Weber, T. (2011). Supramolecular templating in kirromycin biosynthesis: the acyltransferase KirCII loads ethylmalonyl-CoA extender onto a specific ACP of the trans-AT PKS. Chem. Biol. *18*, 438–444.

Musiol, E.M., Greule, A., Härtner, T., Kulik, A., Wohlleben, W., and Weber, T. (2013). The AT_2 domain of KirCI loads malonyl extender units to the ACPs of the kirromycin PKS. ChemBioChem *14*, 1343–1352.

Piel, J. (2010). Biosynthesis of polyketides by trans-AT polyketide synthases. Nat. Prod. Rep. *27*, 996–1047.

Schneidman-Duhovny, D., Inbar, Y., Nussinov, R., and Wolfson, H.J. (2005). PatchDock and SymmDock: servers for rigid and symmetric docking. Nucleic Acids Res. *33* (Web Server issue), W363–W367.

Shan, Q., and Lynch, J.W. (2010). Chimera construction using multiple-template-based sequential PCRs. J. Neurosci. Methods *193*, 86–89.

Staunton, J., and Weissman, K.J. (2001). Polyketide biosynthesis: a millennium review. Nat. Prod. Rep. *18*, 380–416.

Sundermann, U., Bravo-Rodriguez, K., Klopries, S., Kushnir, S., Gomez, H., Sanchez-Garcia, E., and Schulz, F. (2013). Enzyme-directed mutasynthesis: a combined experimental and theoretical approach to substrate recognition of a polyketide synthase. ACS Chem. Biol. *8*, 443–450.

Tang, G.L., Cheng, Y.Q., and Shen, B. (2004). Leinamycin biosynthesis revealing unprecedented architectural complexity for a hybrid polyketide synthase and nonribosomal peptide synthetase. Chem. Biol. *11*, 33–45.

Tang, Y.Y., Kim, C.Y., Mathews, I.I., Cane, D.E., and Khosla, C. (2006). The 2.7-Angstrom crystal structure of a 194-kDa homodimeric fragment of the 6-deoxyerythronolide B synthase. Proc. Natl. Acad. Sci. USA *103*, 11124–11129.

Tang, Y., Chen, A.Y., Kim, C.Y., Cane, D.E., and Khosla, C. (2007). Structural and mechanistic analysis of protein interactions in module 3 of the 6-deoxyerythronolide B synthase. Chem. Biol. *14*, 931–943.

Volkman, B.F., Zhang, Q., Debabov, D.V., Rivera, E., Kresheck, G.C., and Neuhaus, F.C. (2001). Biosynthesis of D-alanyl-lipoteichoic acid: the tertiary structure of apo-D-alanyl carrier protein. Biochemistry *40*, 7964–7972.

Walker, M.C., Thuronyi, B.W., Charkoudian, L.K., Lowry, B., Khosla, C., and Chang, M.C. (2013). Expanding the fluorine chemistry of living systems using engineered polyketide synthase pathways. Science *341*, 1089–1094.

Weber, T., Laiple, K.J., Pross, E.K., Textor, A., Grond, S., Welzel, K., Pelzer, S., Vente, A., and Wohlleben, W. (2008). Molecular analysis of the kirromycin biosynthetic gene cluster revealed beta-alanine as precursor of the pyridone moiety. Chem. Biol. *15*, 175–188.

Weissman, K.J., Hong, H., Popovic, B., and Meersman, F. (2006). Evidence for a protein-protein interaction motif on an acyl carrier protein domain from a modular polyketide synthase. Chem. Biol. *13*, 625–636.

Wong, F.T., Chen, A.Y., Cane, D.E., and Khosla, C. (2010). Protein-protein recognition between acyltransferases and acyl carrier proteins in multimodular polyketide synthases. Biochemistry *49*, 95–102.

Wong, F.T., Jin, X., Mathews, I.I., Cane, D.E., and Khosla, C. (2011). Structure and mechanism of the trans-acting acyltransferase from the disorazole synthase. Biochemistry *50*, 6539–6548.

Zhao, C., Coughlin, J.M., Ju, J., Zhu, D., Wendt-Pienkowski, E., Zhou, X., Wang, Z., Shen, B., and Deng, Z. (2010). Oxazolomycin biosynthesis in Streptomyces albus JA3453 featuring an "acyltransferase-less" type I polyketide synthase that incorporates two distinct extender units. J. Biol. Chem. *285*, 20097–20108.

